Figure S1: Mitochondrial turnover from axon terminals is consistent across all conditions imaged. (**a**) Axon terminals in NM3 (mid-trunk neuromast) at 6 dpf show similar levels of mitochondria turnover to the same terminals 24 hrs after photoconversion at 4 dpf (see Fig. 1; n=23). (**b**,**c**) Terminal cluster neuromast axon terminals show similar levels of mitochondrial turnover after photoconversion at 4 (n=15) and 6 dpf (n=21). (**d**,**e**) Removing the larvae from their agarose chambers between imaging sessions shows similar loss of converted mitochondrial signal at both 4 (n=14) and 6 (n=15) dpf at NM3. (**f**) Motor neuron axons also show mitochondrial turnover within 24 hrs after photoconversion at 4 dpf (n=13). (**g**) Schematic of motor neuron axon photoconversion in the *Tg(neurod:mito-mEos)* transgenic line. (**h**) Images showing the conversion of mitochondria (magenta) and the loss of this signal 24 hrs after conversion in motor neuron axons. For all, ANOVAs with Tukey HSD posthoc contrasts.

Figure S2: Expression of PercevalHR in single motor neuron cell bodies and their axons at 4 dpf. (**a**,**b**) Single motor neuron cell body in *actr10*$^{-}$ mutant and wildtype sibling expressing PercevalHR. (**c**,**d**) Expression of PercevalHR in a single motor neuron axon in a wildtype (**c**) and *actr10*$^{-}$ mutants (**d**) larvae at 4 dpf. Asterisk on autofluorescent pigment cell. Scale bars – 10μm.

Figure S3: ATP SnFR analysis of cytosolic ATP levels at 4 dpf. (**a**-**d**) Expression of *5kbneurod:mRuby-ATPSnFR* in a single wildtype and *actr10*$^{-}$ mutant pLL neuronal cell body and associated axon terminal. (**e**) Schematic of the transient transgenesis used to express the mRuby tagged ATP SnFR in a single neuronal soma and its axon terminal in the pLL system. (**f**) Quantification of the ATP SnFR fluorescence intensity normalized to mRuby expression shows no difference in ATP levels between wildtype and *actr10*$^{-}$ mutant neurons (ANOVA). Sample size indicated on graph. Scale bars – 10μm.

Figure S4: Rescued *actr10*$^{-}$ mutant HCs effectively mechanotransduce upon stimulation but show inhibited synaptic responses. (**a**) Schematic of the neuromast indicating the Apex of the stereocilia where mechanotransduction takes place and the Base of the hair cell where the pre-synapse is located. (**b**,**c**) Wildtype and *actr10*$^{-}$ mutant HC rescue transgenic zebrafish larvae at 5 dpf show active mechanotransduction in HC stereocilia (Apex). (**b`**,**c`**) Heat map of Apex GCaMP6s fluorescence intensity changes with stimulation. (**d**,**e**) Quantification of the change in GCaMP6s fluorescence intensity showing active mechanotransduction in both wildtype and HC rescued *actr10*$^{-}$ mutants. (**f**,**g**) *actr10*$^{-}$ HC rescue mutants show reduced calcium influx at the presynapse. (**f`**,**g`**) Heat map of GCaMP6s fluorescence intensity changes at the HC base with stimulation. (**h**,**i**) Quantification of the change in GCaMP6s fluorescence intensity upon stimulation (*t*-test). Sample size indicated on graph. Scale bar – 10μm.

Figure S5: Immunolabeling of proteins identified in the mass spectrometry analysis as decreased in *actr10*$^{-}$ mutant mitochondria. (**a**-**d**) Immunofluorescence of ZZEF1 in the pLLg and axon terminals. (**e**-**h**) Immunofluorescence of Rps26 in the pLLg and axon terminals. (**i-p**) Immunolabeling of two proteins not altered in the mitochondrial mass spec data set, LamC and Aldh6a. Immunofluorescence signal in the pLLg was isolated from surrounding tissue using the ImageJ *Image calculator* tool for image preparation. Arrowheads point to a region of the axon terminal for each. Scale bar – 10μm.

Figure S1

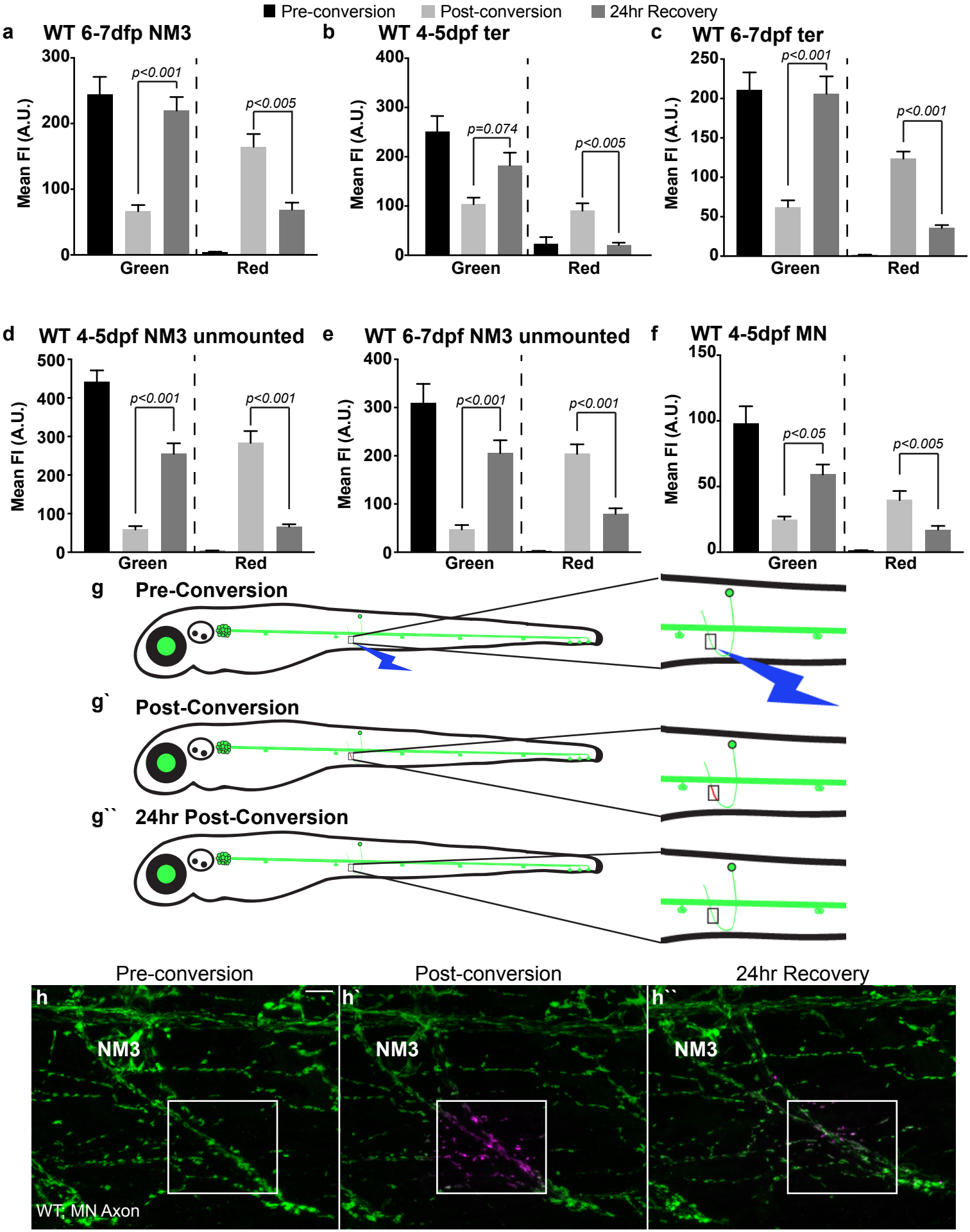
Pre-conversion
Post-conversion
24hr Recovery
a
WT 6-7dfp NM3
b
WT 4-5dpf ter
c
WT 6-7dpf ter
d
WT 4-5dpf NM3 unmounted
e
WT 6-7dpf NM3 unmounted
f
WT 4-5dpf MN
Mean FI (A.U.)
Green
Red
p<0.001
p<0.005
p=0.074
p<0.05
g
Pre-Conversion
g`
Post-Conversion
g``
24hr Post-Conversion
Pre-conversion
Post-conversion
24hr Recovery
h
h`
h``
NM3
WT; MN Axon

Figure S2

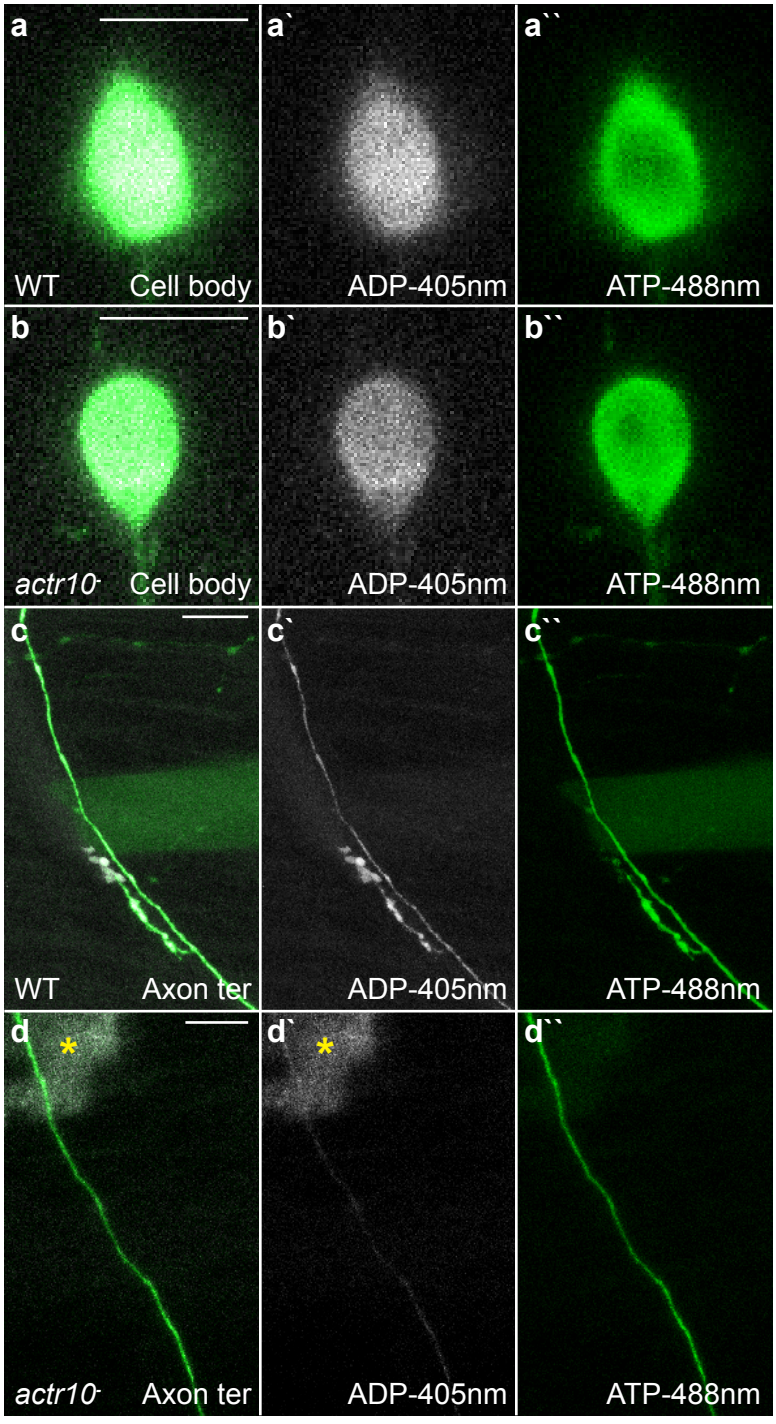
a
a`
a``
WT
Cell body
ADP-405nm
ATP-488nm
b
b`
b``
actr10-
Cell body
ADP-405nm
ATP-488nm
c
c`
c``
WT
Axon ter
ADP-405nm
ATP-488nm
d
d`
d``
*
*
actr10-
Axon ter
ADP-405nm
ATP-488nm

Figure S3

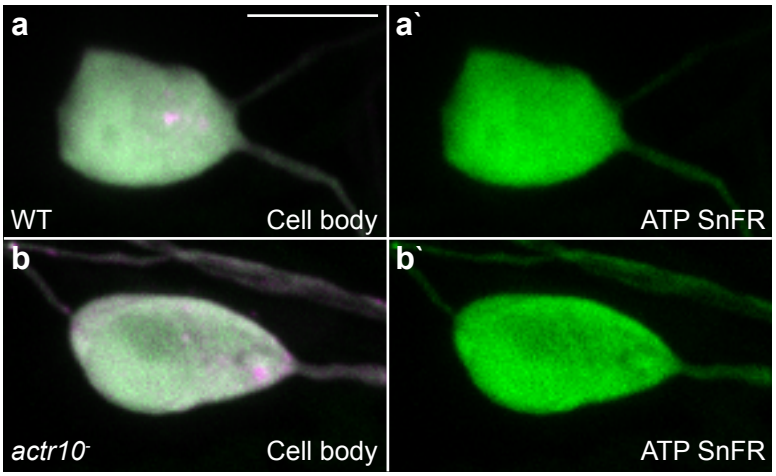
a
a`
WT
Cell body
ATP SnFR
b
b`
actr10-
Cell body
ATP SnFR

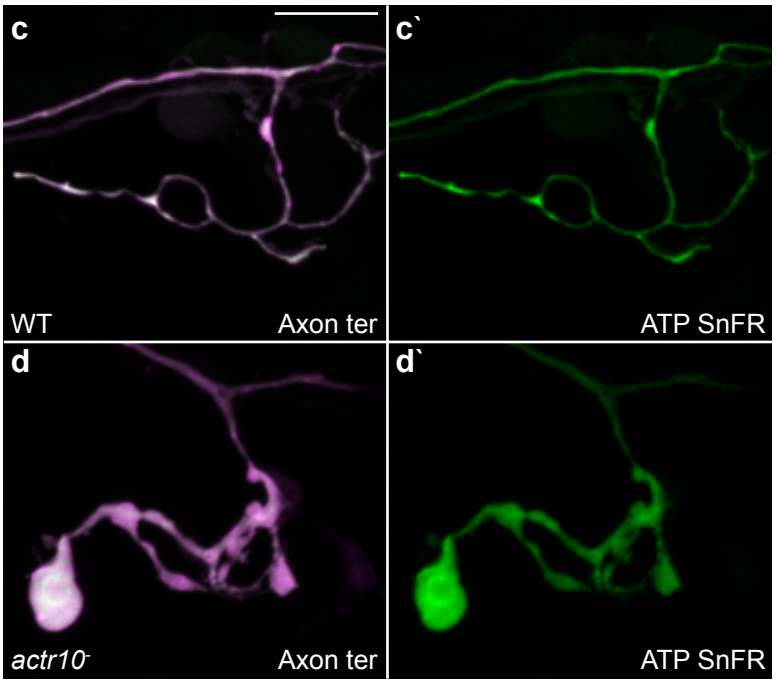
c
c`
WT
Axon ter
ATP SnFR
d
d`
actr10-
Axon ter
ATP SnFR

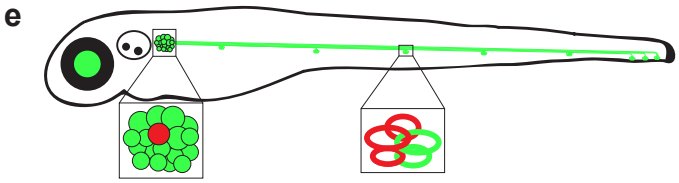
e

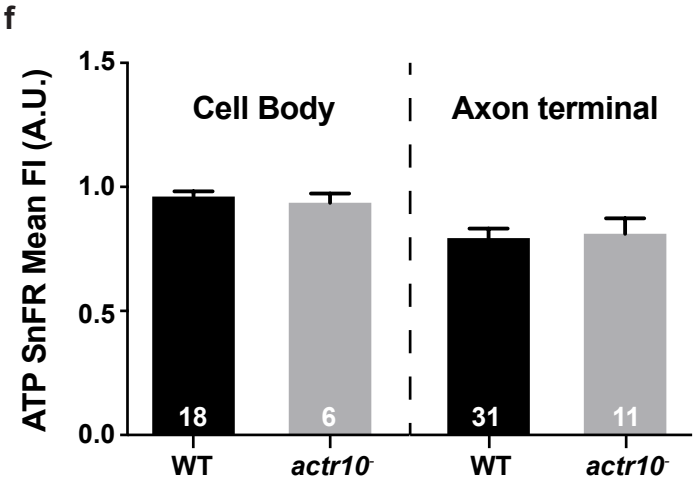
f
ATP SnFR Mean FI (A.U.)
1.5
1.0
0.5
0.0
Cell Body
Axon terminal
18
6
31
11
WT
actr10-
WT
actr10-

Figure S4

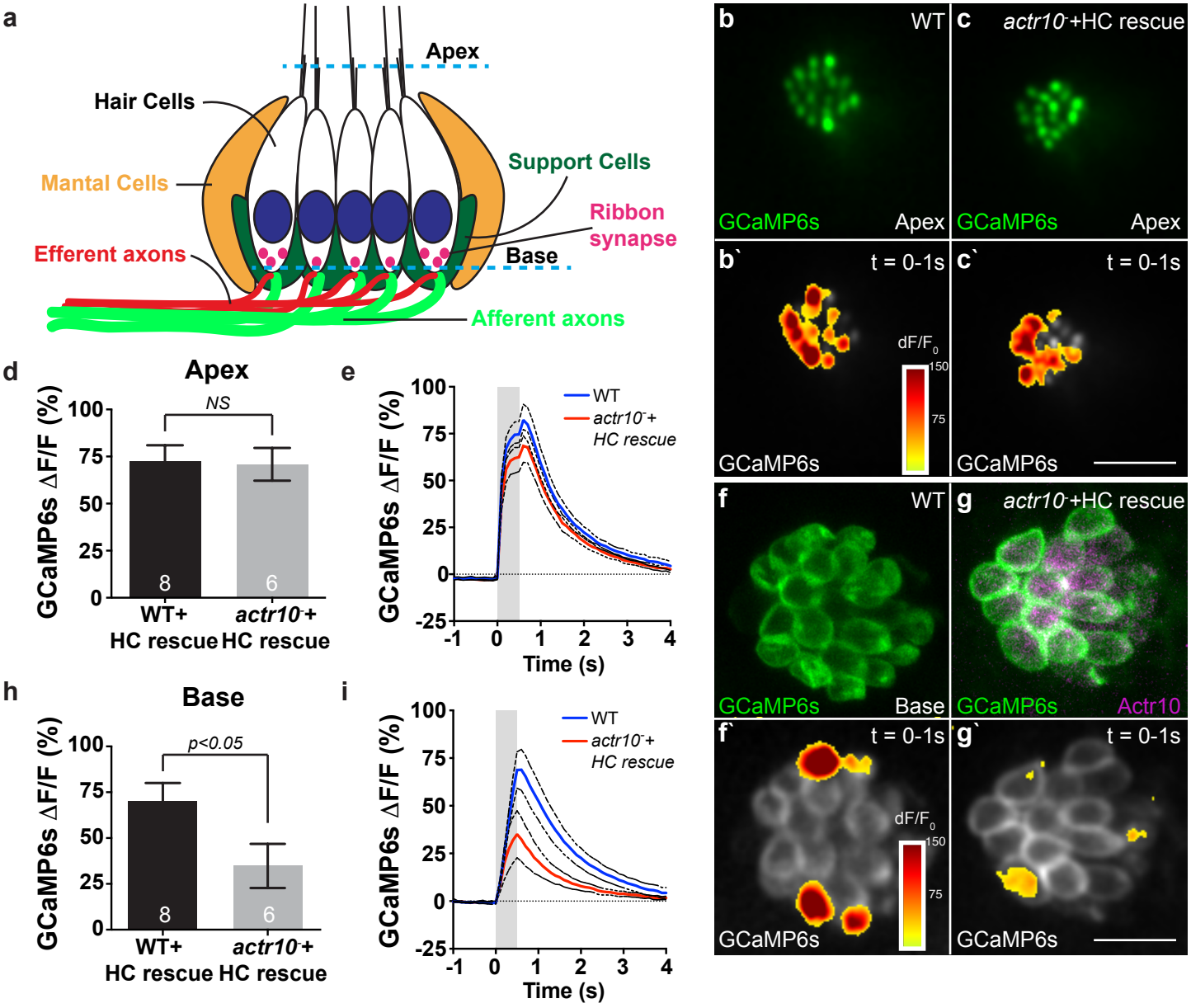
a
Apex
Hair Cells
Mantal Cells
Support Cells
Ribbon synapse
Efferent axons
Base
Afferent axons
b
WT
GCaMP6s
Apex
c
actr10-+HC rescue
GCaMP6s
Apex
b`
t = 0-1s
dF/F0
150
75
GCaMP6s
c`
t = 0-1s
GCaMP6s
d
Apex
NS
GCaMP6s ΔF/F (%)
100
75
50
25
0
8
6
WT+ HC rescue
actr10-+ HC rescue
e
GCaMP6s ΔF/F (%)
WT
actr10-+ HC rescue
-25
-1
0
1
2
3
4
Time (s)
f
WT
GCaMP6s
Base
g
actr10-+HC rescue
GCaMP6s
Actr10
f`
t = 0-1s
dF/F0
150
75
GCaMP6s
g`
t = 0-1s
GCaMP6s
h
Base
p<0.05
GCaMP6s ΔF/F (%)
100
75
50
25
0
8
6
WT+ HC rescue
actr10-+ HC rescue
i
GCaMP6s ΔF/F (%)
WT
actr10-+ HC rescue
-25
-1
0
1
2
3
4
Time (s)

Figure S5

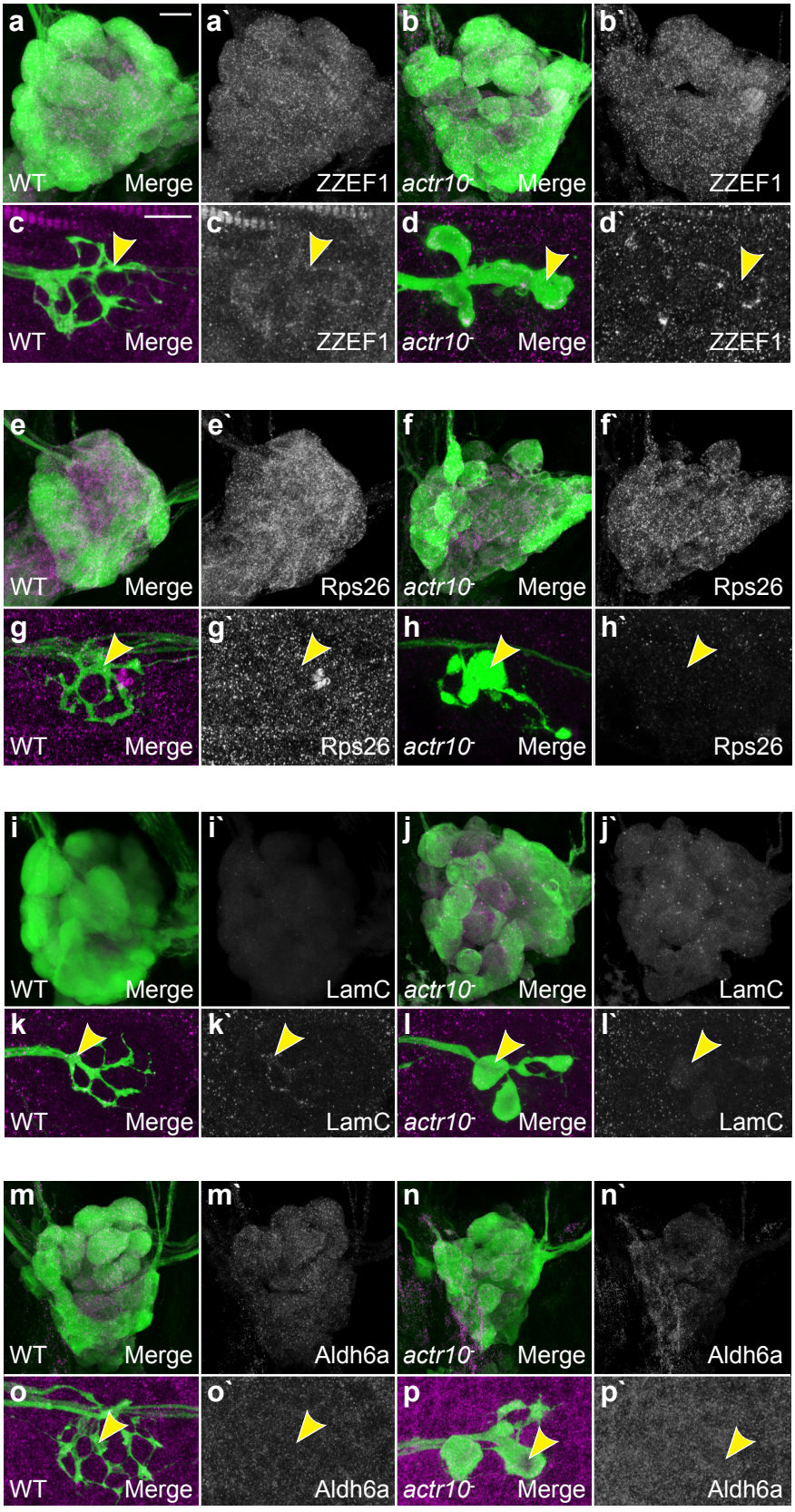
a
a`
b
b`
WT
Merge
ZZEF1
actr10-
Merge
ZZEF1
c
c`
d
d`
WT
Merge
ZZEF1
actr10-
Merge
ZZEF1
e
e`
f
f`
WT
Merge
Rps26
actr10-
Merge
Rps26
g
g`
h
h`
WT
Merge
Rps26
actr10-
Merge
Rps26
i
i`
j
j`
WT
Merge
LamC
actr10-
Merge
LamC
k
k`
l
l`
WT
Merge
LamC
actr10-
Merge
LamC
m
m`
n
n`
WT
Merge
Aldh6a
actr10-
Merge
Aldh6a
o
o`
p
p`
WT
Merge
Aldh6a
actr10-
Merge
Aldh6a

Reagents or Resources	Source	Catalog number
Zebrafish Strains		
AB	ZIRC	ZL1
actr10^{nl15}	(Drerup et al., 2017)	NA
p150b^{nl16}	(Drerup et al., 2017)	NA
TgBAC(neurod:egfp)^{nl1}	(Obholzer et al., 2008)	NA
Tg(5kbneurod:mito-mEos)^{y568}	(Mandal et al., 2018)	NA
Tg(5kbneurod:G-GECO)^{nl19}	(Mandal et al., 2018)	NA
Tg(5kbneurod:mito-R-GECO)^{nl20}	(Mandal et al., 2018)	NA
Tg(myo6b:mRFP-actr10)^{y610}	This paper	NA
Tg(-6myo6b:GCaMP6s-CAAX)^{idc1Tg}	(Sheets et al., 2017)	NA
Tg(hsp70l:GCaMP6s-CAAX-SiLL1)^{idc8Tg}	(Zhang et al., 2018)	NA
Antibodies for IF		
GFP; 1:2000	Aves	GFP-1020
DsRed; 1:1000	ThermoFisher	632496
Apex1; 1:100	DSHB	CPTC-Apex1-2-s
ZZEF1; 1:500	ThermoFisher	PA5-56856
Sod2; 1:500	ThermoFisher	PA1-31072
RPS15a; 1:100	ThermoFisher	PA5-24733
RPS26; 1:500	ThermoFisher	PA5-85689
RPL27; 1:200	ThermoFisher	PA5-51728
Tom20; 1:200	Santa Cruz	sc-11415
Ribeye b; 1:10,000	(Sheets et al., 2011)	NA
MAGUK; 1:500	NeuroMab	K28/86
Myosin7a; 1:1000	Proteus Biosciences	25-6790
AlexFluor 488/568/647; 1:1000	ThermoFisher	assorted
Antibodies for Western blot		
LC3; 1:2000	Novus	NB100-2331SS
GFP; 1:2500	ThermoFisher	A11122
Anti-rabbit*HRP	Jackson Immunoresearch	711-036-152
Drug Treatments		
Pepstatin A; 10μm	Fisher Scientific	BP26715
E-64-D; 10μm	Enzo Life Sciences	BML-PI107-0001
Vital Dyes		
Tetramethylrhodamine ethyl ester (TMRE)	ThermoFisher	T669
FM1-43	ThermoFisher	T35356

Genotyping target	Forward Primer	Reverse Primer
actr10^{nl15}	TGTTTTCGGATGAACTGCCTG	CGTGTAGGCCGCTCCTAAAT
p150a	TAGTGTGCAGATCCAATATGGC	ATTTCCCAGAGGCGAAGAGT
p150b^{nl16}	TCGGCTTCTGCAGGAGAGAT	CTGGGTCCCGGGATTGGAG
Tg(myo6b:mRFP-actr10)^{y610}	CGCCTACAAGACCGACATCA	TGGACATCAGGTGACTGGGA

Construct	Citation	Sensor original source
5kbneurod:mito-TagRFP	(Drerup et al., 2017)	(Fang et al., 2012)
5kbneurod:mito-TIMER	(Mandal et al., 2018)	Addgene: 50547
5kbneurod:PercevalHR-mCherryCAAX	(Mandal et al., 2018)	Addgene: 49082

5kbneurod:roGFP2	This paper	Addgene: 64977
5kbneurod:mito-roGFP2	This paper	Addgene: 64977
5kbneurod:mRuby-ATPSnFR	This paper	Lobas et al 2019
mnx1:PercevalHR-mCherryCAAX	This paper	Addgene: 49082

shRNA against Rat Actr10	**Sequence**
#1	ggcatgtctaagccgatcaaa
#2	ggtcctggattgtggatatag
#3	gtgcttggatcaatcagagat

References

Drerup, C.M., Herbert, A.L., Monk, K.R., and Nechiporuk, A.V. (2017). Regulation of mitochondria-dynactin interaction and mitochondrial retrograde transport in axons. Elife *6*.

Fang, C., Bourdette, D., and Banker, G. (2012). Oxidative stress inhibits axonal transport: implications for neurodegenerative diseases. Mol Neurodegener *7*, 29.

Mandal, A., Pinter, K., and Drerup, C.M. (2018). Analyzing Neuronal Mitochondria in vivo Using Fluorescent Reporters in Zebrafish. Front Cell Dev Biol *6*, 144.

Obholzer, N., Wolfson, S., Trapani, J.G., Mo, W., Nechiporuk, A., Busch-Nentwich, E., Seiler, C., Sidi, S., Sollner, C., Duncan, R.N.*, et al.* (2008). Vesicular glutamate transporter 3 is required for synaptic transmission in zebrafish hair cells. J Neurosci *28*, 2110-2118.

Sheets, L., He, X.J., Olt, J., Schreck, M., Petralia, R.S., Wang, Y.X., Zhang, Q., Beirl, A., Nicolson, T., Marcotti, W.*, et al.* (2017). Enlargement of Ribbons in Zebrafish Hair Cells Increases Calcium Currents But Disrupts Afferent Spontaneous Activity and Timing of Stimulus Onset. J Neurosci *37*, 6299-6313.

Sheets, L., Trapani, J.G., Mo, W., Obholzer, N., and Nicolson, T. (2011). Ribeye is required for presynaptic Ca(V)1.3a channel localization and afferent innervation of sensory hair cells. Development *138*, 1309-1319.

Zhang, Q., Li, S., Wong, H.C., He, X.J., Beirl, A., Petralia, R.S., Wang, Y.X., and Kindt, K.S. (2018). Synaptically silent sensory hair cells in zebrafish are recruited after damage. Nat Commun *9*, 1388.